RSC Advances

COMMUNICATION

View Article Online
View Journal | View Issue

CrossMark click for updates

Cite this: *RSC Adv.*, 2015, **5**, 7729

Received 5th November 2014
Accepted 10th December 2014

DOI: 10.1039/c4ra13906b

www.rsc.org/advances

Three-dimensional TiO_2/CeO_2 nanowire composite for efficient formaldehyde oxidation at low temperature†

Yongchao Huang, Haibo Li, Muhammad-Sadeeq Balogun, Hao Yang, Yexiang Tong, Xihong Lu* and Hongbing Ji*

We developed a low-cost and high-performance TiO_2/CeO_2 nanowire-based catalyst for efficient catalytic volatile organic compound oxidation at low temperature. The TiO_2/CeO_2 nanowires yield a remarkable HCHO conversion efficiency of 60.2% at a low temperature of 60 °C and have excellent catalytic stability as well as good activity for toluene oxidation.

The ever-increasing demands for human health have stimulated extensive attention on the quality of indoor air because people usually spend more than 80% of their time in houses and offices.[1–3] Formaldehyde (HCHO), a typical volatile organic compound (VOC), is a major indoor air pollutant that is released from the urea–formaldehyde insulation finishing materials, particle board, sealants and oil paint.[4–6] Long term exposure to HCHO may cause serious health problems, such as irritation of eyes and the respiratory tract, headache, pneumonia, and even lung and nasopharyngeal cancer.[7] Numerous efforts have been devoted to removing the indoor HCHO, and some strategies have been proposed in the recent years.[8–10] One of the most effective methods is to convert HCHO into CO_2 and H_2O over catalysts *via* low-temperature thermal catalytic oxidation in terms of its low cost, environmentally friendly reaction conditions and energy saving.[11] To improve the efficiency and reduce the reaction temperature of the thermal catalytic HCHO oxidation, considerable attention has focused on the design and synthesis of high-performance catalysts. Noble metal-based catalysts, such as supported Pt,[7,12–14] Pd[15,16] and Au[17,18] on transition metal oxides containing Mn, Ce, Ti and Cu have been extensively explored as catalysts and proven to show excellent catalytic performance for HCHO oxidation at relatively low temperatures. For example, complete oxidation of HCHO over noble metals/metal oxide-based catalysts occurs above 150 °C over Ru/CeO_2,[19] $Ag/MnO_x–CeO_2$,[20] above 50–100 °C over Au/CeO_2,[21] and above 80 °C over Au/FeO_x [17] and Pt/TiO_2.[14] Recent studies have shown that HCHO can be completely oxidized on $Au/CeO_2–Co_3O_4$ [18] and Pt/TiO_2 [13,14] catalysts near/at room temperature. Liu *et al.* developed a kind of macroporous $Au/CeO_2–Co_3O_4$ catalyst that can completely oxidize HCHO at a low temperature of 39 °C.[22] Nie *et al.* reported a NaOH-modified Pt/TiO_2 catalyst for room-temperature catalytic oxidation of HCHO.[7] However, the scarcity and expensive nature of noble metals severely hinder their practical application as catalysts. The development of alternate low-cost and effective catalysts for HCHO oxidation at room/low temperature is highly desirable.

In this study, we focused on the development of a high-performance and non-precious metal catalyst based on one-dimensional (1D) low cost metal oxide nanowires. In comparison to bulk materials and nanoparticles, nanowires can provide a larger interfacial area and shorter diffusion path for active species, and thus hold great promise for catalysts. Here, we report a novel TiO_2/CeO_2 nanowire composited catalyst for low-temperature combustion of HCHO without any precious metal. The synergistic effects from CeO_2, TiO_2, and 1D structure enable the TiO_2/CeO_2 nanowires to possess superior catalytic activity and stability for HCHO oxidation at low temperature. It could convert 60.2% of HCHO at a low temperature of 60 °C, which is not achieved by any non-precious metal based catalysts at such a low temperature. The as-prepared TiO_2/CeO_2 nanowire composite exhibited excellent catalytic stability as well as good activity for toluene oxidation. Furthermore, the catalytic activity of the TiO_2/CeO_2 nanowire composite could be remarkably enhanced after loading 1 wt% Pt nanoparticles (NPs), which was able to completely oxidize HCHO to CO_2 and H_2O at room temperature (20 °C) and toluene at about 250 °C.

Fig. 1a presents the growth process of the 1D TiO_2/CeO_2 nanowire catalyst. First, free-standing TiO_2 nanowires were grown on flexible carbon cloth substrate by a seed-assisted

Department of Chemical Engineering, MOE of the Key Laboratory of Bioinorganic and Synthetic Chemistry, School of Chemistry and Chemical Engineering, The Key Lab of Low-carbon Chemistry, Energy Conservation of Guangdong Province, Sun Yat-Sen University, Guangzhou 510275, People's Republic of China. E-mail: luxh6@mail.sysu.edu.cn; jihb@mail.sysu.edu.cn; Fax: +86 2084112245

† Electronic supplementary information (ESI) available: Synthetic details, experimental details and additional descriptions, figures. See DOI: 10.1039/c4ra13906b

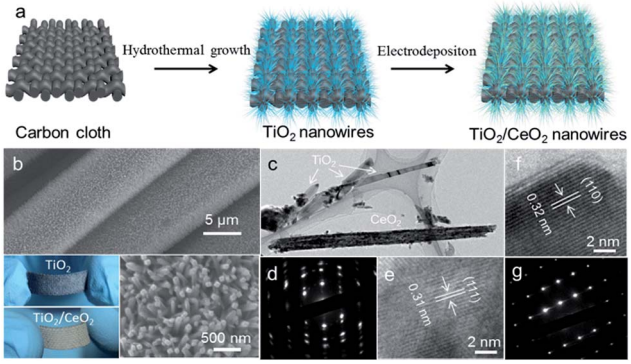

Fig. 1 (a) Schematic diagram illustrating the growth process of TiO_2/CeO_2 nanowires on carbon cloth. (b) SEM and optical images of the as-prepared TiO_2/CeO_2 nanowires on carbon cloth. (c) TEM image of TiO_2/CeO_2 nanowires. (d) SAED pattern and (e) HRTEM image of CeO_2 nanowire that recorded from CeO_2 nanowire in (c). (g and f) HRTEM image and SAED pattern of TiO_2 nanowire that recorded from TiO_2 nanowire in (c).

hydrothermal method reported elsewhere (see the Experimental section).[23] Scanning electron microscopy (SEM) images revealed that the carbon fibers were uniformly covered with TiO_2 nanowires (Fig. S1a†). The average diameter of these as-grown TiO_2 nanowires is about 100–200 nm and their lengths are around 2 μm (Fig. S1b†). An X-ray diffraction (XRD) spectrum collected for TiO_2 nanowires confirms the tetragonal structure of the rutile TiO_2 (JCPDF # 65-0192) (Fig. S2†). Then, CeO_2 nanowires were deposited onto the TiO_2 nanowires by anodic electrodeposition at different time variation (15–120 min) (with optimized catalytic performance at 90 min) (Experimental section, ESI†). After CeO_2 electrodeposition, the white color of TiO_2 film turned into light yellow-white (bottom in Fig. 1b). SEM studies reveal that the morphology of nanowires was mostly preserved but distributed more closely (Fig. 1b), suggesting the CeO_2 nanowires were grown between the spaces of TiO_2 nanowires. The successful growth of CeO_2 nanowires was confirmed by XRD spectra (Fig. S2†). Besides the diffraction peaks of rutile TiO_2 (JCPDS # 88-1175), the diffraction peaks of cubic CeO_2 (JCPDS # 65-2975) are clearly observed, showing the presence of CeO_2 in TiO_2/CeO_2 nanowires.

Transmission electron microscopy (TEM) analyses were conducted to study the detailed microstructures of TiO_2/CeO_2 nanowires. Fig. 1c displays a typical TEM image of TiO_2/CeO_2 nanowires, from which the TiO_2 nanowires and CeO_2 nanowires can be clearly identified. The surface of TiO_2 nanowires is very smooth while the surface of CeO_2 nanowires is relatively rough. Selected-area electron diffraction (SAED) analyses reveal that the CeO_2 nanowire has poly-crystalline structure (Fig. 1d) and TiO_2 nanowire has single crystalline structure (Fig. 1g). Fig. 1e is a high-resolution TEM (HRTEM) image of the CeO_2 nanowire (Fig. 1c), again confirming the poly-crystalline nature of CeO_2 nanowire. The measured lattice fringe spacing is about 0.31 nm, which is consistent with the *d*-spacing of (111) planes of cubic CeO_2 (JCPDS # 65-2975). A HRTEM image collected from the TiO_2 nanowire reveals clear lattice fringes with a lattice fringe spacing of 0.32 nm, which is in agreement with the *d*-spacing of (110) planes of rutile TiO_2 (Fig. 1f). These data disclose that the TiO_2/CeO_2 nanowires are not core–shell nanowires but composites of TiO_2 nanowires and CeO_2 nanowires. Furthermore, X-ray photoelectron spectroscopy (XPS) analysis further confirms that the composition of the composite nanowires is TiO_2 and CeO_2 (Fig. S3†). All these results reveal the successful fabrication of TiO_2/CeO_2 nanowire composite.

Catalytic oxidation of HCHO was carried out to evaluate the catalytic performance of the TiO_2/CeO_2 nanowire catalysts. For comparison, pristine TiO_2 nanowires and CeO_2 nanowires were also studied. Pristine CeO_2 nanowires were directly grown on carbon cloth by the same electrodeposition method with TiO_2/CeO_2 nanowires (Experimental section, ESI†). SEM and XRD analyses confirm that cubic CeO_2 nanowires with a diameter of 150 nm were uniformly coated on the carbon cloth surface (Fig. S4†). Fig. 2a shows the conversion efficiency of HCHO to CO_2 as a function of temperature over the TiO_2 nanowires, CeO_2 nanowires and TiO_2/CeO_2 nanowires. By analyzing these data, several features are worth noting. First, the gradual increase in the conversion efficiency with increasing reaction temperature

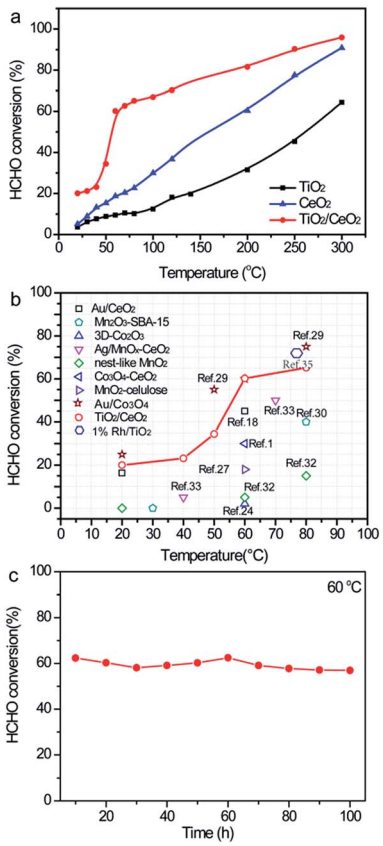

Fig. 2 (a) Catalytic performance of HCHO over TiO_2 nanowires, CeO_2 nanowires and TiO_2/CeO_2 nanowires as a function of temperature under the following conditions: HCHO concentration = 50 ppm, 25 vol% O_2, N_2 as balance gas, hourly space velocity (GSHV) = 30 000 mL h^{-1} g^{-1}. (b) The comparison of HCHO conversion efficiencies of our TiO_2/CeO_2 nanowires with the recently reported catalysts.[18,24,27,29–33] (c) Catalytic performance of HCHO over TiO_2/CeO_2 nanowires at 60 °C as a function of time.

indicates that HCHO is more easily oxidized over these samples at high temperature. The HCHO conversion efficiency of the TiO_2/CeO_2 nanowires is much higher than the pristine TiO_2 nanowires and CeO_2 nanowires in the entire temperature windows, confirming the superior catalytic activity of the TiO_2/CeO_2 nanowires. Second, at a low temperature of 20 °C, approximately 20% of HCHO could be converted over the TiO_2/CeO_2 nanowires, while only 3% and 4% for pristine TiO_2 nanowires and CeO_2 nanowires, respectively. Third, with the reaction temperature increased to 60 °C, the TiO_2/CeO_2 nanowires yielded a remarkably higher HCHO conversion efficiency of 60.2%, whereas the TiO_2 and CeO_2 nanowires only achieved 9.5% and 18.8%, respectively, at the same temperature. Moreover, such low reaction temperature for 60% HCHO conversion obtained for TiO_2/CeO_2 nanowires is substantially lower than the values recently reported for most of non-precious catalysts[24–27] and some precious catalysts,[14,17] such as 3D-Co_3O_4 (110 °C),[24] and MnO_2/cellulose (120 °C),[27] MnO_x–CeO_2 (80 °C),[25] $Mn_xCo_{3-x}O_4$ (65 °C),[26] Au/CeO_2 (70 °C),[17] 1% Rh/TiO_2 (75 °C).[14] Fig. 2b compares the HCHO conversion efficiencies of our TiO_2/CeO_2 nanowires with other reported catalysts at low temperature ranging from 20 to 80 °C. Significantly, the HCHO conversion performances of the TiO_2/CeO_2 nanowires at low temperatures are substantially higher than most reported no-precious catalysts, and even comparable to the previously reported precious catalysts, such as Au/CeO_2 [17,21] and Ag/MnO_x–CeO_2.[20] All the above results fully validate that the TiO_2/CeO_2 nanowires possess significantly high catalytic activity for HCHO oxidation at low temperature.

Beside the conversion efficiency, the long-term stability of the catalyst is also very important for their practical applications. To evaluate the catalytic stability of the TiO_2/CeO_2 nanowires, the catalytic oxidation performance of HCHO over TiO_2/CeO_2 nanowires on stream at 60 °C for 100 h is shown in Fig. 2c. Impressively, the TiO_2/CeO_2 nanowires exhibited a remarkable long-term catalytic stability with only less than 3% decrease in HCHO conversion efficiency after 100 h. Fig. S5a† displays the TG curve of TiO_2/CeO_2 nanowires performed in air flow from 35 to 900 °C. Less than 2% of mass loss was observed for the TiO_2/CeO_2 nanowires below 600 °C, indicating the excellent thermal stability of TiO_2/CeO_2 nanowires between 35 to 600 °C. SEM observations reveal that the morphology of the TiO_2/CeO_2 nanowires was preserved after 100 h long-test (Fig. S5b†). Additionally, XRD (Fig. S5c†) and XPS (Fig. S5d†) survey spectra confirm that there were no obvious changes in the phase and chemical composition of TiO_2/CeO_2 nanowires after testing for 100 h. Thus, the remarkable stability of the TiO_2/CeO_2 nanowires is due to their excellent thermal strength, morphology and phase stability as well as flexible free-standing carbon cloth, which could offer high mechanical stability.

To gain insights into the reasons for the excellent catalytic performance of TiO_2/CeO_2 nanowires, the H_2-temperature-programmed reduction (TPR) analysis was carried out. Fig. 3a compares the H_2-TPR profiles of the TiO_2, CeO_2 and TiO_2/CeO_2 samples. The pristine CeO_2 nanowires exhibited two reduction peaks, and the low-temperature reduction peak located at 485 °C is attributed to the reduction of surface capping oxygen of

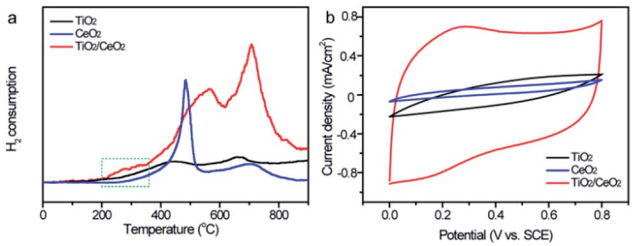

Fig. 3 (a) H_2-TPR profiles of the TiO_2 nanowires, CeO_2 nanowires and TiO_2/CeO_2 nanowires. (b) CV curves of the TiO_2 nanowires, CeO_2 nanowires and TiO_2/CeO_2 nanowires obtained at a scan rate of 100 mV s^{-1}.

CeO_2, while the high-temperature reduction peak at 708 °C is ascribed to the lattice oxygen of CeO_2.[28] Reduction of TiO_2 alone is more difficult and essentially no TPR peak was observed from 30 to 750 °C. Importantly, significant enhancement in the reducibility was observed for the TiO_2/CeO_2 composite sample. A new reduction peak (marked by green dash rectangle) occurred in the range from 200 to 350 °C, which is attributed to the synergistic effect of CeO_2 and TiO_2 nanowires. This reduction peak makes the major contribution to HCHO oxidation in comparison with the other two reduction peaks in the high temperature region around 560 °C and 708 °C. In general, the lower temperature of the corresponding desorption peak centered at the 200–350 °C range indicates that it is easier to generate surface active oxygen species, which may offer a higher catalytic activity in oxidation reactions. The lowering of reduction temperature implies that the presence of CeO_2 helps to weaken the surface oxygen on TiO_2/CeO_2 nanowires, and therefore improves the reducibility of the catalyst.

Cyclic voltammogram (CV) curves of the pristine TiO_2 nanowires, CeO_2 nanowires and TiO_2/CeO_2 nanowires collected at a scan rate of 100 mV s^{-1} in HCHO (40%) aqueous electrolyte are displayed in Fig. 3b. All the samples showed approximately rectangle-like shapes, revealing the electric double layer capacitance characteristic. The substantially higher current density of the TiO_2/CeO_2 sample over the pristine TiO_2 and CeO_2 samples show that it possesses larger surface area. The specific surface area of the pristine TiO_2, CeO_2, and TiO_2/CeO_2 samples is about 18.3, 24.4 and 36.7 m^2 g^{-1}, respectively. Given the experimental results above, two possible reasons are proposed to explain the significantly enhanced catalytic performance of the TiO_2/CeO_2 nanowires. First, a good interfacial contact between CeO_2 and TiO_2 nanowires would form legitimately, which could allow HCHO to be absorbed easily. In addition, CeO_2 is rich in oxygen vacancy defects and has a large oxygen storage capacity, which is beneficial for the HCHO catalytic oxidation. Second, the free-standing 1D nanowires grown on carbon cloth not only offer a large surface area for surface reactions, but also enable the fast transport of species and extend the reaction sites from the surface to the subsurface of the catalysts. In order to study the optimizational ratio of the CeO_2 on the TiO_2 nanowires, we deposited CeO_2 on the TiO_2 nanowires at different durations and studied their catalytic performance, which are shown in Fig. S6.† Significantly,

depositing CeO_2 on the TiO_2 nanowires for 60 and 90 min gave closely related performance.

Our as-prepared TiO_2/CeO_2 nanowires also have excellent catalytic activity for toluene combustion. Fig. 4 shows the conversion efficiency of toluene (1000 ppm) to CO_2 as a function of temperature over the TiO_2/CeO_2 nanowires at the gas hourly space velocity = 60 000 mL h^{-1} g^{-1}. It is worth pointing out that CO_2 and H_2O were the only products. Significantly, the TiO_2/CeO_2 nanowires catalyst could convert 50% of the toluene at 170 °C and achieved complete toluene conversion at above 300 °C. The present temperatures of TiO_2/CeO_2 sample at 170 °C and 300 °C for 50% and 100% of toluene conversion, respectively, are substantially lower and comparable to the values obtained from previously reported catalysts at similar reaction conditions, such as wire-like MnO_2 (50% at 225 °C),[34] MnO_2–KIT6 (50% at 203 °C),[35] NiO–CTAB-2 (50% at 256 °C),[36] $LaMnO_3$ (50% at 193 °C),[37] mesoporous $LaFeO_3$ (50% at 200 °C),[38] K_xMnO_2 nanospheres (50% at 209 °C),[39] Ag–Mn/SBA-15 (50% at 202 °C),[40] $Eu_{1-x}Sr_xFeO_3$ (50% at 278 °C).[41]

In addition to being used as catalyst, the free-standing 1D structure of TiO_2/CeO_2 nanowires also enables them to serve as a good support for noble metals to achieve VOC oxidation at lower temperatures. Here, we examined the feasibility of TiO_2/CeO_2 nanowires to support Pt nanoparticles for HCHO and toluene oxidation. Pt nanoparticles with a mass loading of about 1% were prepared on the surface of the TiO_2/CeO_2 nanowires by a reduction method (Experiment section, ESI†). A SEM image shows that the smooth surface of TiO_2/CeO_2 nanowires became relatively rough after Pt nanoparticle coating (Fig. S7a†). The TEM observation clearly shows that well crystalline Pt nanoparticles were uniformly coated on the nanowire surface, which is further confirmed by the EDS elemental mapping (Fig. S7b†). As expected, the $Pt/TiO_2/CeO_2$ nanowires achieved complete HCHO conversion at room temperature, which could convert more than 99% of HCHO to CO_2 at 20 °C. This present efficiency is substantially higher than or comparable to the values of the recently reported 1 wt% Pt/TiO_2 catalyst (14.3% at 20 °C),[14] 2 wt% Pt/nest-like MnO_2 catalyst (24.3% at 20 °C),[32] Au/Co_3O_4–CeO_2 (75.2% at 25 °C),[18] Pt/γ-Al_2O_3 (100% at 25 °C),[12] Pd–Mn/Al_2O_3 (100% at 90 °C),[15] Pt/f-SiO_2 (100% at 25 °C),[42] 1 wt% Pd/TiO_2 (95.5% at 25 °C),[16] 1 wt% Na–1 wt% Pt/TiO_2 (100% at 40 °C)[43] and slightly lower than those of $LaMnO_3$ (100% at 200 °C)[44] and 6.5-Au/meso-Co_3O_4 (100% at 190 °C).[45] Furthermore, the $Pt/TiO_2/CeO_2$ catalyst also showed remarkably enhanced catalytic activity compared to the TiO_2/CeO_2 catalyst toward toluene oxidation that could achieve 50% toluene conversion at 120 °C and complete conversion at 250 °C.

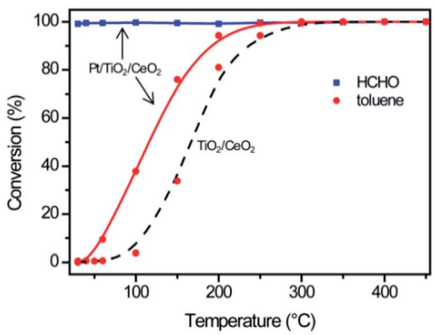

Fig. 4 Catalytic performances of HCHO and toluene over TiO_2/CeO_2 nanowires and $Pt/TiO_2/CeO_2$ nanowire samples as a function of temperature.

Conclusions

In summary, we have demonstrated the feasibility of flexible 3D TiO_2/CeO_2 nanowires as a new and high-performance catalyst for low-temperature thermal catalytic oxidation of HCHO. The as-prepared TiO_2/CeO_2 nanowires exhibited superior catalytic activity that could convert 60.2% of HCHO to CO_2 and H_2O at a low temperature of 60 °C, which is the best performance ever reported for non-precious metal based catalysts at such a low temperature. Additionally, the TiO_2/CeO_2 nanowires had an outstanding long-term cycling stability without any decay of its catalytic activity after 100 h, and also showed a good catalytic activity toward toluene oxidation. Furthermore, the TiO_2/CeO_2 nanowires were proved to be excellent supports for noble metals to achieve VOCs oxidation at lower temperatures. After loading with 1% Pt NPs, the $Pt/TiO_2/CeO_2$ nanowires were able to completely oxidize HCHO at room temperature (20 °C) and toluene at about 250 °C. This work offers a new insight to design low-cost and high-efficiency catalysts for low-temperature thermal catalytic oxidation of VOCs.

Acknowledgements

We acknowledge the financial support of this work by the Natural Science Foundations of China (21036009, 21273290 and 91323101), the Research Fund for the Doctoral Program of Higher Education of China (20120171110043) and the Young Teacher Starting-up Research program of Sun Yat-Sen University.

Notes and references

1 C. Y. Ma, Z. Mu, J. J. Li, Y. G. Jin, J. Cheng, G. Q. Lu, Z. P. Hao and S. Z. Qiao, *J. Am. Chem. Soc.*, 2010, **132**, 2608–2613.
2 Z. Jin, P. Li, G. Liu, B. Zheng, H. Yuan and D. Xiao, *J. Mater. Chem. A*, 2013, **1**, 14736–14743.
3 C. Zhang, P. Zhang, S. Li, G. Wu, X. Ma and J. Gong, *Phys. Chem. Chem. Phys.*, 2012, **14**, 3295–3298.
4 S. Wang, B. Xiao, T. Yang, P. Wang, C. Xiao, Z. Li, R. Zhao and M. Zhang, *J. Mater. Chem. A*, 2014, **2**, 6598–6604.
5 R. Rao, M. Yang, C. Li, H. Dong, S. Fang and A. Zhang, *J. Mater. Chem. A*, 2015, **3**, 782–788.
6 H. Huang, D. Y. Leung and D. Ye, *J. Mater. Chem.*, 2011, **21**, 9647–9652.
7 L. Nie, J. Yu, X. Li, B. Cheng, G. Liu and M. Jaroniec, *Environ. Sci. Technol.*, 2013, **47**, 2777–2783.
8 S. Arrii, F. Morfin, A. J. Renouprez and J. L. Rousset, *J. Am. Chem. Soc.*, 2004, **126**, 1199–1205.

9 D. Tang, Z. Chen, J. Hu, G. Sun, S. Lu and C. Hu, *Phys. Chem. Chem. Phys.*, 2012, **14**, 12829–12837.
10 Q. Yuan, Z. Wu, Y. Jin, L. Xu, F. Xiong, Y. Ma and W. Huang, *J. Am. Chem. Soc.*, 2013, **135**, 5212–5219.
11 X. Tang, J. Chen, X. Huang, Y. Xu and W. Shen, *Appl. Catal., B*, 2008, **81**, 115–121.
12 L. Nie, A. Meng, J. Yu and M. Jaroniec, *Sci. Rep.*, 2013, **3**, 3215–3220.
13 L. Wang, M. Sakurai and H. Kameyama, *J. Hazard. Mater.*, 2009, **167**, 399–405.
14 C. Zhang, H. He and K.-i. Tanaka, *Appl. Catal., B*, 2006, **65**, 37–43.
15 M. Álvarez-Galván, B. Pawelec, V. D. l. Peña O'Shea, J. Fierro and P. Arias, *Appl. Catal., B*, 2004, **51**, 83–91.
16 H. Huang and D. Y. C. Leung, *ACS Catal.*, 2011, **1**, 348–354.
17 C. Li, Y. Shen, M. Jia, S. Sheng, M. O. Adebajo and H. Zhu, *Chem. Commun.*, 2008, 355–361.
18 C. Ma, D. Wang, W. Xue, B. Dou, H. Wang and Z. Hao, *Environ. Sci. Technol.*, 2011, **45**, 3628–3634.
19 S. Imamura, Y. Uematsu, K. Utani and T. Ito, *Ind. Eng. Chem. Res.*, 1991, **30**, 18–21.
20 X. Tang, J. Chen, Y. Li, Y. Li, Y. Xu and W. Shen, *Chem. Eng. J.*, 2006, **118**, 119–125.
21 Y. Shen, X. Yang, Y. Wang, Y. Zhang, H. Zhu, L. Gao and M. Jia, *Appl. Catal., B*, 2008, **79**, 142–148.
22 B. Liu, Y. Liu, C. Li, W. Hu, P. Jing, Q. Wang and J. Zhang, *Appl. Catal., B*, 2012, **127**, 47–58.
23 X. Lu, M. Yu, G. Wang, T. Zhai, S. Xie, Y. Ling, Y. Tong and Y. Li, *Adv. Mater.*, 2013, **25**, 267–272.
24 B. Bai, H. Arandiyan and J. Li, *Appl. Catal., B*, 2013, **142**, 677–683.
25 X. Liu, J. Lu, K. Qian, W. Huang and M. Luo, *J. Rare Earths*, 2009, **27**, 418–424.
26 C. Shi, Y. Wang, A. Zhu, B. Chen and C. Au, *Catal. Commun.*, 2012, **28**, 18–22.
27 L. Zhou, J. He, J. Zhang, Z. He, Y. Hu, C. Zhang and H. He, *J. Phys. Chem. C*, 2011, **115**, 16873–16878.
28 S. Watanabe, X. Ma and C. Song, *J. Phys. Chem. C*, 2009, **113**, 14249–14257.
29 M. Jia, H. Bai, Y. Shen and Y. Li, *Mesoporous Mater.*, 2008, **26**, 528–531.
30 R. Averlant, S. Royer, J. M. Giraudon, J. P. Bellat, I. Bezverkhyy, G. Weber and J. F. Lamonier, *ChemCatChem*, 2014, **6**, 152–161.
31 X. Tang, J. Chen, Y. Li, Y. Li, Y. Xu and W. Shen, *Chem. Eng. J.*, 2006, **118**, 119–125.
32 X. Yu, J. He, D. Wang, Y. Hu, H. Tian and Z. He, *J. Phys. Chem. C*, 2011, **116**, 851–860.
33 B. Liu, Y. Liu, C. Li, W. Hu, P. Jing, Q. Wang and J. Zhang, *Appl. Catal., B*, 2012, **127**, 47–58.
34 F. Wang, H. Dai, J. Deng, G. Bai, K. Ji and Y. Liu, *Environ. Sci. Technol.*, 2012, **46**, 4034–4041.
35 Y. Du, Q. Meng, J. Wang, J. Yan, H. Fan, Y. Liu and H. Dai, *Microporous Mesoporous Mater.*, 2012, **162**, 199–206.
36 G. Bai, H. Dai, J. Deng, Y. Liu, W. Qiu, Z. Zhao, X. Li and H. Yang, *Chem. Eng. J.*, 2013, **219**, 200–208.
37 C. Zhang, Y. Guo, Y. Guo, G. Lu, A. Boreave, L. Retailleau, A. Baylet and A. Giroir-Fendler, *Appl. Catal., B*, 2014, **148–149**, 490–498.
38 B. Gao, J. Deng, Y. Liu, Z. Zhao, X. Li, Y. Wang and H. Dai, *Chin. J. Catal.*, 2013, **34**, 2223–2229.
39 H. Chen, J. He, C. Zhang and H. He, *J. Phys. Chem. C*, 2007, **111**, 18033–18038.
40 Z. Qu, Y. Bu, Y. Qin, Y. Wang and Q. Fu, *Appl. Catal., B*, 2013, **132–133**, 353–362.
41 K. Ji, H. Dai, J. Deng, H. Jiang, L. Zhang, H. Zhang and Y. Cao, *Chem. Eng. J.*, 2013, **214**, 262–271.
42 N. An, W. Zhang, X. Yuan, B. Pan, G. Liu, M. Jia, W. Yan and W. Zhang, *Chin. J. Catal.*, 2013, **215**, 1–6.
43 C. Zhang, F. Liu, Y. Zhai, H. Ariga, N. Yi, Y. Liu, K. Asakura, M. Flytzani-Stephanopoulos and H. He, *Angew. Chem., Int. Ed.*, 2012, **51**, 9628–9632.
44 C. Zhang, Y. Guo, Y. Guo, G. Lu, A. Boreave, L. Retailleau, A. Baylet and A. Giroir-Fendler, *Appl. Catal., B*, 2014, **148–149**, 490–498.
45 Y. Liu, H. Dai, J. Deng, S. Xie, H. Yang, W. Tan, W. Han, Y. Jiang and G. Guo, *J. Catal.*, 2014, **309**, 408–418.